VERSITA

OPTO-ELECTRONICS REVIEW **18**(2), 155–162

DOI: 10.2478/s11772-010-0007-x

Comparative analysis of interferogram noise filtration using wavelet transform and spin filtering algorithms

B. ZIELINSKI* and K. PATORSKI

Institute of Micromechanics and Photonics, Warsaw University of Technology, 8 Św. Andrzeja Boboli Str., 02-525 Warsaw, Poland

The aim of this paper is to analyze 2D fringe pattern denoising performed by two chosen methods based on quasi-1D two-arm spin filter and 2D discrete wavelet transform (DWT) signal decomposition and thresholding. The ultimate aim of this comparison is to estimate which algorithm is better suited for high-accuracy measurements by phase shifting interferometry (PSI) with the phase step evaluation using the lattice site approach. The spin filtering method proposed by Yu et al. (1994) was designed to minimize possible fringe blur and distortion. The 2D DWT also presents such features due to a lossless nature of the signal wavelet decomposition. To compare both methods, a special 2D histogram introduced by Gutman and Weber (1998) is used to evaluate intensity errors introduced by each of the presented algorithms.

Keywords: interferometry, fringe analysis, spatial filtering.

1. Introduction

Within the last couple of decades, a number of algorithms designed for the automatic interferogram phase retrieval has been proposed. The underlying phase-encoded physical parameters being measured can be determined by one of the temporal or spatial methods [1].

The phase stepping interferometry (PSI) method requires at least three interferograms of the same phase distribution, each phase-shifted in reference to the base interferogram. The method enables us to perform very precise measurements as the phase value in every pixel is computed independently. Linear and nonlinear phase step errors, nonlinear detection, quantization and noise errors are the major sources limiting the measurement accuracy. On the other hand, correct application of the Fourier-transform method, most frequently used spatial technique, relies upon either a correct choice of the bandpass filter or almost noiseless interferograms, depending on a specific implementation used.

In view of the above facts, it is readily understood that the interferogram noise reduction is an important issue which affects entire area of interferometric measurements. It also justifies vast amount of denoising algorithms being developed over the past years. Two classes of denoising methods have emerged as the leading ones. The first one utilizes outstanding capabilities of a wavelet transform in both continuous and discrete variants to denoise 1D or 2D signals [2]. The other class, called spin filtering, is based on the fact that signal and noise in a 2D fringe pattern can be easily separated in 1D neighbourhood if the noise is in a different frequency band than the signal [3,4]. To achieve this, the fringe tangent direction in every point of a fringe pattern is estimated.

The aim of this paper is to study 2D fringe pattern denoising performed by the two chosen methods, one using quasi-1D two-arm spin filter and the other using a 2D discrete wavelet transform (DWT) signal decomposition and thresholding. The ultimate aim of this comparison is to estimate which algorithm is better suited for high-accuracy interferometric measurements performed by the phase shifting interferometry (PSI) method, aided with the phase step determination using the so-called lattice site approach. In spite of the fact that both algorithms are designed to minimize possible fringe blur and distortion, the evaluation of the errors introduced by each algorithm is essential for proper estimation of their performance.

The overall assessment is divided into several parts. At first, the artificial fringe pattern with Gaussian-distribution noise is generated to acquire more insight into the wavelet transform denoising. Then, both denoising algorithms are applied to filter out the fringe pattern recorded in the experiment. Finally, the statistical analysis of the differences between the original and denoised patterns permits to draw conclusions based on unwanted influence introduced by each algorithm. For this purpose, the lattice site approach originally proposed for inspecting the phase shifter calibration has been adopted.

This work represents an extension of previously published studies on the application of the lattice site method to quantitative assessment of experimental errors encountered in the phase shifting interferometry [5,6].

*e-mail: b.zielinski@mchtr.pw.edu.pl

2. Spin filter denoising

Spin filtering is a denoising technique developed by Yu [3] later extended, among many others, by Yu and co-workers [4]. The spin filtering method relies on the fact that the intensity of a fringe pattern in the direction tangential to the fringes contains almost only noise, so in this case the noise can be isolated from the signal of interest. Therefore the main condition of the effective denoising is fulfilled. The main filtering scheme is explained below with a particular emphasis put on the implementation details.

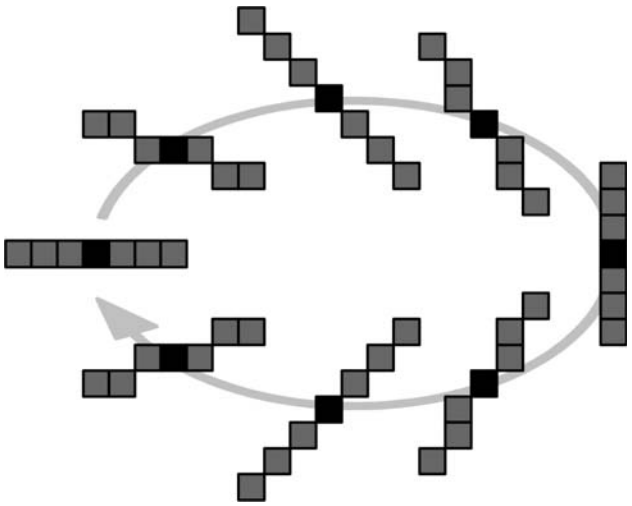

Fig. 1. Predefined directions used in case of a 7×7 filter size. Black square represents pixel under analysis. "Spinning" of the analysis direction can be observed.

2.1. Algorithm description

For every pixel in an interferogram, its neighbourhood (user-defined range) is analyzed. In this neighbourhood, a tangential direction to the fringe direction is estimated. Acquiring the line of the least gradient is the most crucial part of the algorithm. Two different ways of solving this problem have been developed. One relies on checking eight predefined directions and determining the direction with the smallest gradient (see Fig. 1).

The second solution uses plane fitting to a matrix of neighbourhood intensity values to determine the locally tangential direction to the analyzed fringes, i.e., the spin direction. An estimation of the plane coefficients by least squares method enables us to not only find the tangential direction of a plane but most importantly the locus of the least gradient. In the final step, intensities comprising the above mentioned line are used to compute a new intensity value for an analyzed pixel, either by calculating a mean value or a median. After a new intensity value is computed, the analysis is moved to the next pixel.

2.2. Properties of the used methods

One of the main sources of error of the spin filtering scheme originates from a silent assumption that the fringe part being analyzed is straight, any curvature introduces errors and this fact is affecting both approaches in the same manner. The other factor complementing the overall error is an inaccurately estimated line of the least gradient. Certainly, this type of error impacts the most the first implementation, where the predefined directions are used. The second approach is more universal than the first one, because the neighbourhood scope can be user-defined whereas in the first one this important parameter is fixed. On the other hand, much simpler architecture of the first approach results in fast execution time in contrast to the second, much more computation-intensive method.

3. Wavelet denoising

Wavelet processing is the latest concept aimed at solving the problem of the non-stationary signal analysis.

One of the most significant disadvantages of standard Fourier analysis is its global character. For instance, if an extra term with very small amplitude will be added to a sine

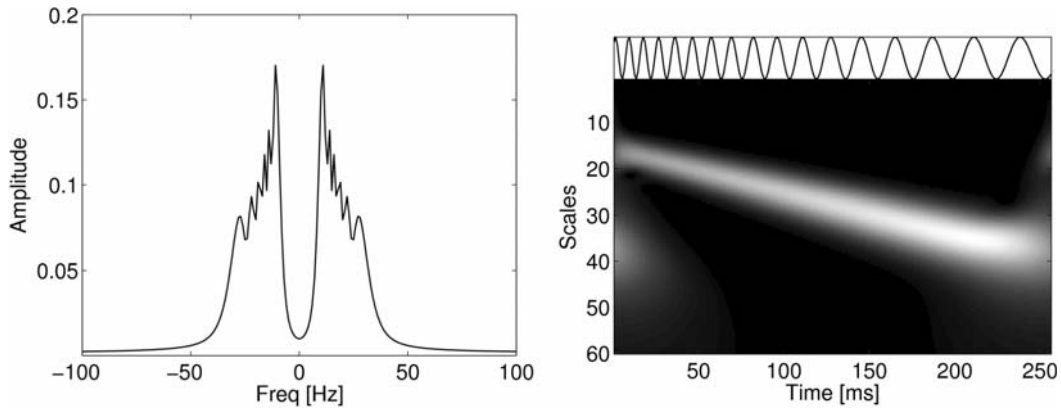

Fig. 2. Examples of wavelet and Fourier transforms of the same linear chirp signal (artificially generated signal with linearly changing frequency, length 256 ms, 1024 samples). FFT spectrum showing a blurred peak – a band of mean frequencies of a signal (on the left). CWT of this signal (computed using Morlet mother wavelet with the parameters $k_0 = 6$, $\sigma = 1$, after Ref. 7), clearly showing instantaneous frequency for every point of it due to time-scale localization (on the right). Intensity of image corresponds to a local value of a wavelet coefficient.

wave, the overall signal will hardly be modified but its Fourier spectrum will change significantly. It is commonly known that in this transform the whole time information about the signal is transformed into its frequency spectrum. To overcome this limitation, a concept of windowed Fourier transform (WFT) has been developed [8], where the signal is divided into parts, and then each of them is frequency-analyzed using a Fourier transform. The outcome is visualized on a plane of time-frequency "atoms" (a spectrogram) where each point corresponds to a WFT coefficient.

The real-life signals tend to have low frequency content for longer periods of time and brief moments of high frequency content [9]. The transform that uses the same window size for all analyzed frequencies is surely non-optimal, for the low frequencies the analysis window will be too short, whereas for the high frequencies it will be too long.

The wavelet transform addresses this by adjusting the width of the analysis window to each scale, the lower the frequency band being analyzed, the wider is the window. Due to a more general approach to a signal (e.g., it is not time-based) in the wavelet analysis, the term scale is used instead of frequency, those parameters are inversely proportional to each other. Just like in the WFT, the scale-time relationship of a signal is represented as a 2D plane – the scalogram. The exemplary result of applying both of the transforms to one signal is shown in Fig. 2.

3.1. From continuous WT to discrete WT

In case of the CWT, the signal is convolved with wavelets of different scales. A wavelet at each scale corresponds to a certain bandwidth being analyzed. If the wavelet filter bank chosen is not orthogonal, then a portion of spectrum that is analyzed at a given scale will partially overlap with the ones computed using the neighbouring scales, this leads to unnecessary calculations and data redundancy. To avoid it, the orthogonal wavelet filter banks are used to extend CWT into the discrete wavelet transform (DWT), where the entire frequency axis is covered with non-overlapping wavelet spectra of increasing bandwidth, in that way the redundancy is minimized.

3.2. Inverse WT

A reconstruction formula can be used to invert the wavelet transformation exactly if only the wavelet used has a zero mean and a finite energy. When those conditions are fulfilled, the inverse WT is then just a linear superposition of the wavelets at a given time and scale with its corresponding coefficients.

3.3. Algorithm description

Fringe pattern wavelet denoising scheme used in this article is based on a principle of coefficient thresholding. An image is decomposed using 2D DWT, utilizing Daubechies mother-wavelet of the fifth order. This ensures that the wavelet fully reconstructs any signal that locally fits in a space of the fourth order polynomials [10]. Then all coefficient values from every scale are compared with a computed threshold given by the equation [11]:

$$Th = C(2\log n)^{1/2}, \tag{1}$$

where n is the number of analyzed samples and C is the median of coefficients on level 1 of a wavelet pyramid. Then, the standard procedure of soft thresholding is applied.

After such processing, the changed wavelet spectrum is synthesized to form a new, noise-suppressed signal. This denoising procedure is proved to be almost optimal in terms of mean squared error over a wide range of signal classes [11].

4. Performance comparison

The performance comparison of both the algorithms will be conducted using two sets of fringe patterns, one artificially generated and the other using experimental data. Sample images are presented in Fig. 3. Note that modulation in case of the artificially generated pattern is equal to ±90 grey levels. This means that after adding 10% of modulation value, Gaussian-type noise, the extreme values still fit within an 8-bit greyscale.

To compare the performance of both algorithms in an experiment, a special set of interferograms has been chosen. Figure 3(c) shows the example of interferometric measurement of a vibrating membrane [12]. The image is characterized by two features, wide bandwidth of spatial frequencies (there are areas with high and low fringe densities near the membrane edges and its centre, respectively) and highly varying fringe modulation (that directly corresponds to local amplitude of vibrations, see a close-up in Figs. 3(c) and 3(d)). Those two attributes make such an interferogram a perfect proving ground for all algorithms that are supposed to work in a wide range of interferogram parameters.

4.1. "Qualitative" method

Selected set of five interferograms, where the first one is treated as a reference and the other four are phase-shifted by 90 degrees, is denoised. Both of the examined algorithms are applied to individual frames and the results are saved. To emphasize the demerits of the confronted algorithms for their performance assessment the following equation is used:

$$Mod(x,y) = \frac{1}{2}\sqrt{\left|[I_2(x,y) - I_4(x,y)]^2 - [I_1(x,y) - I_3(x,y)]\cdot[I_3(x,y) - I_5(x,y)]\right|}, \tag{2}$$

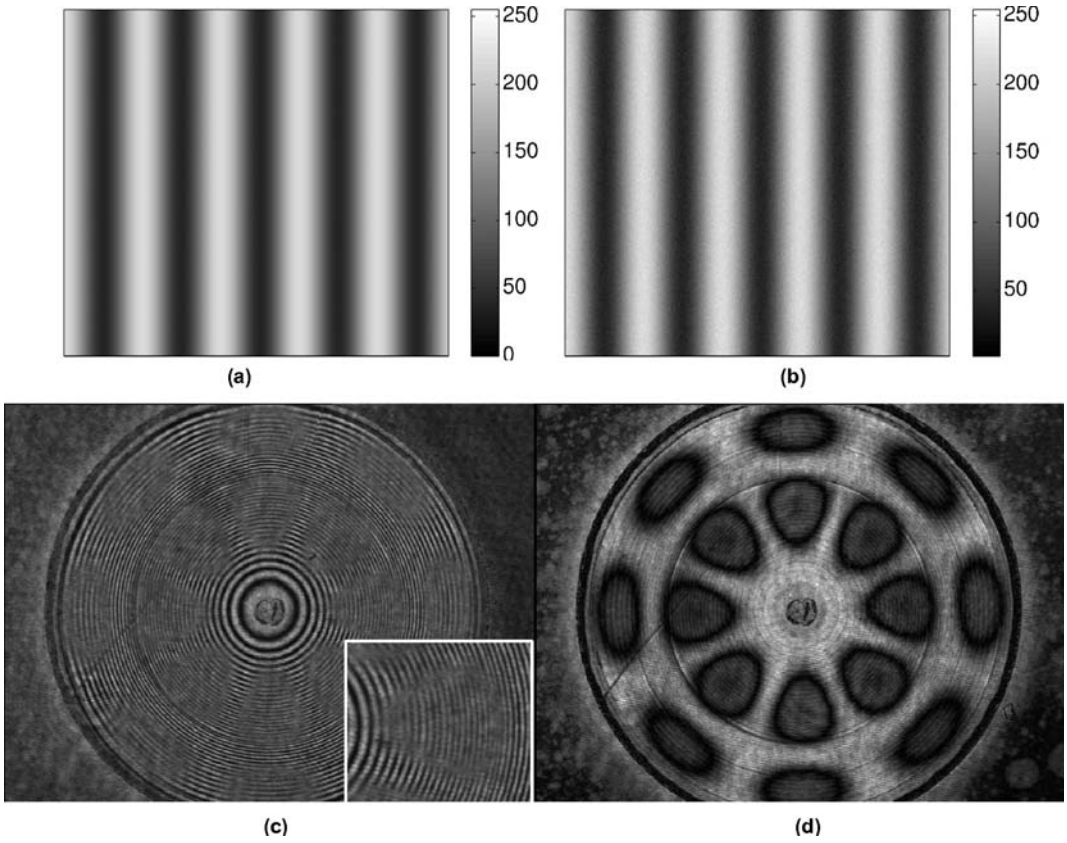

Fig. 3. Simulated fringe images used for numerical analysis: (a) noiseless (ideal) reference, (b) the same image with added noise (10% of fringe modulation value), (c) time-average interferogram of a vibrating membrane used for the experimental verification of algorithm performance with a close-up showing the Bessel function fringe modulation, and (d) modulation map of the interferogram shown in (c) (after Ref. 13).

where Mod is the modulation value for given pixel coordinates, and I_n is the intensity of the n^{th} frame at a given pixel coordinate. This formula has been derived from a temporal phase shifting method and enables one to obtain the map of interferogram modulation [13–16]. Such a map is then confronted with the modulation of an unfiltered data to draw the conclusions concerning the performance of the algorithms.

4.2. Quantitative method

Due to the fact that interferograms used have highly varying features, basic methods of quantitative comparison such as mean and standard deviation of a selected line do not necessarily expose real merits and shortcomings of the examined methods. They tend to be related more to a 1D line than a 2D area. That is why a new comparison methodology has been proposed. Its main principle is based on a paper by Gutman and Weber [17] where a novel method of inspecting a phase-shifter calibration quality by extending the idea of a mean phase-shift angle histogram (routinely used in such cases) to a special 2D histogram – the lattice site – was proposed. The lattice site approach was recently applied to determine other phase shifting experimental errors, e.g., nonlinear recording and tilt-shift errors [5,6].

The most frequent schema of the lattice site approach starts with computing the mean phase-shift angle for a set of interferograms for all pixel coordinates by using the equation [18,19]:

$$\cos\varphi_{av}(x,y) = \frac{1}{2}\frac{I_5(x,y) - I_1(x,y)}{I_4(x,y) - I_2(x,y)} = \frac{Z(x,y)}{M(x,y)}. \qquad (3)$$

Typically, after computing the arccosine of Eq. (3), the histogram is framed where the most frequent angle value is

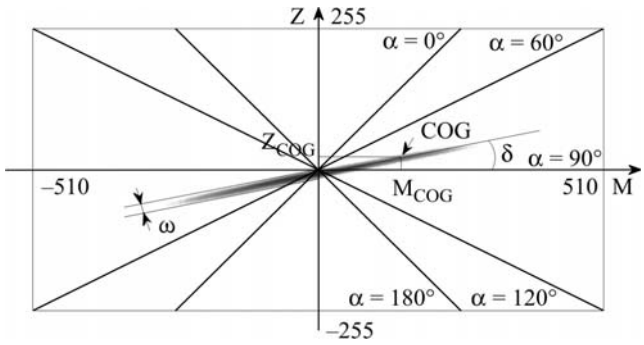

Fig. 4. Lattice site representation of shift angles (after Ref. 17). Z axis corresponds to a numerator of Eq. (3) and M axis to its denominator. The parameter δ corresponds through Eq. (4), to a mean phase-shift angle. (M_{COG}, Z_{COG}) point is the coordinate of a centre of gravity of lattice site positive half, ω corresponds to a width of a representation. The darker the point, the more frequent (M, Z) combination occurs.

believed to be the mean phase-shift angle. In lattice site, however, both parts of the quotient are treated as coordinates to be visualized on a 2D lattice (this term is used since the computed values are contained in a discrete set), see Fig. 4. The (M, Z) combination that corresponds to the denominator and nominator values of Eq. (3) is estimated at every pixel coordinate and then marked on a grid. The grey level of each point is related to the frequency of the given combination, in the sense that the point is darker as the combination is more frequent.

Usually, after the lattice site is constructed, the mean phase-shift angle is computed from the δ value using such relationship:

$$\varphi_{av} = \arccos[\tan(\delta)]. \tag{4}$$

In this case, however, two other important parameters will be sought, the distance between both positive and negative centres of gravity and the ω value. Both of them will be explained further in this paragraph.

The positive centre of gravity (COG) coordinates is computed using the equations below [17]

$$M_{COG+} = \frac{\sum_{M>0}\sum_{Z} M \times H(M,Z)}{\sum_{M>0}\sum_{Z} H(M,Z)}, \qquad Z_{COG+} = \frac{\sum_{M>0}\sum_{Z} Z \times H(M,Z)}{\sum_{M>0}\sum_{Z} H(M,Z)}, \tag{5}$$

where H(M,Z) corresponds to the number of occurrences of a given combination. The negative centre of gravity is calculated similarly. In the end, the distance between those two centres is calculated using a standard length of a vector formula. This parameter is suitable to assess bandwidth dampening of a filtering technique, this distance shrinks while such dampening occurs.

To obtain the parameter ω (see Fig. 4), both positive and negative COG coordinates need to be known. At first, the parameters of a line joining those two coordinates are calculated (the parameters a and b in $y = ax + b$ formula). Then, for every combination occurring at least once throughout the lattice site construction scheme, its distance d from the line mentioned above is evaluated using the formula:

$$d(P,k) = \frac{|Ax_P + By_P + C|}{\sqrt{A^2 + B^2}}, \tag{6}$$

where the point P has the coordinates (x_P,y_P), and the line k is defined as $Ax + By + C = 0$. To obtain meaningful value of the representation width, the ω value, the weighted average of distances is computed with the number of occurrences as a weight. This parameter enables one to assess the denoising capability of the algorithms with high accuracy and in a statistically robust way.

5. Numerical and experimental results

5.1. The issue of WT decomposition level

Before presenting the experimental results, some aspects of the wavelet decomposition, mentioned in Sect. 3.3 need further clarification. Such a decomposition starts with sending a signal through low pass and high pass filters simultaneously. The filters are strictly related to each other. In this way, first (or level 1) approximations (A_1) and details (D_1) are acquired. Then, level 1 approximations are treated in the same way, giving level 2 approximations and details (A_2 and D_2) while D_1 remains unprocessed. In case of this paper, the procedure is repeated to a certain decomposition level, the procedure of determining such level is presented below.

To estimate the optimum level of decomposition for a given data a simulation had to be made. The fringe pattern shown in Fig. 3(a) has been generated and then, after adding a noise [Fig. 3(b)] the data was ready for analysis. The procedure started with estimating global threshold level and then, step-by-step decomposition was made, together with its analysis. The results are presented in Fig. 5 where for every decomposition level, a standard deviation of the picture has been computed. It is clearly seen that in this case the best decomposition will be the one that is performed up to level 4.

The knowledge about this critical point enables us to perform denoising of experimental data with high confidence of the optimum denoising procedure and that is exactly what has been done.

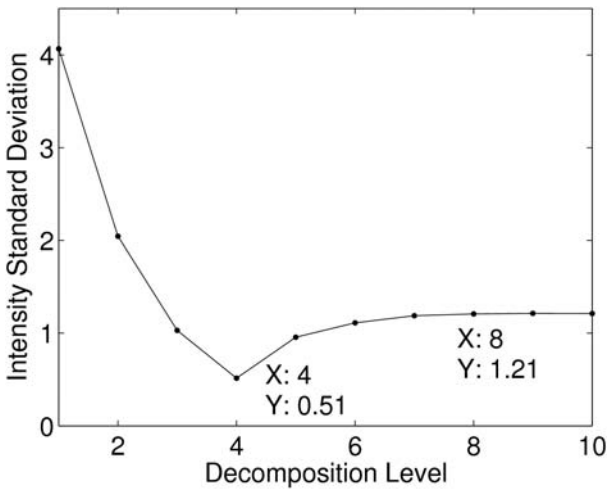

Fig. 5. Intensity standard deviation depending on a decomposition level used. Note the characteristic critical point on a curve which clearly defines the optimum decomposition level [data from Fig. 3(b) were used for calculations].

5.2. Experimental results

The exemplary experimental data shown in Fig. 3(c) is actually a part of the bigger set of interferograms that are denoised using both the spin filter algorithms and the wavelet denoising scheme. The lattice site representation is then

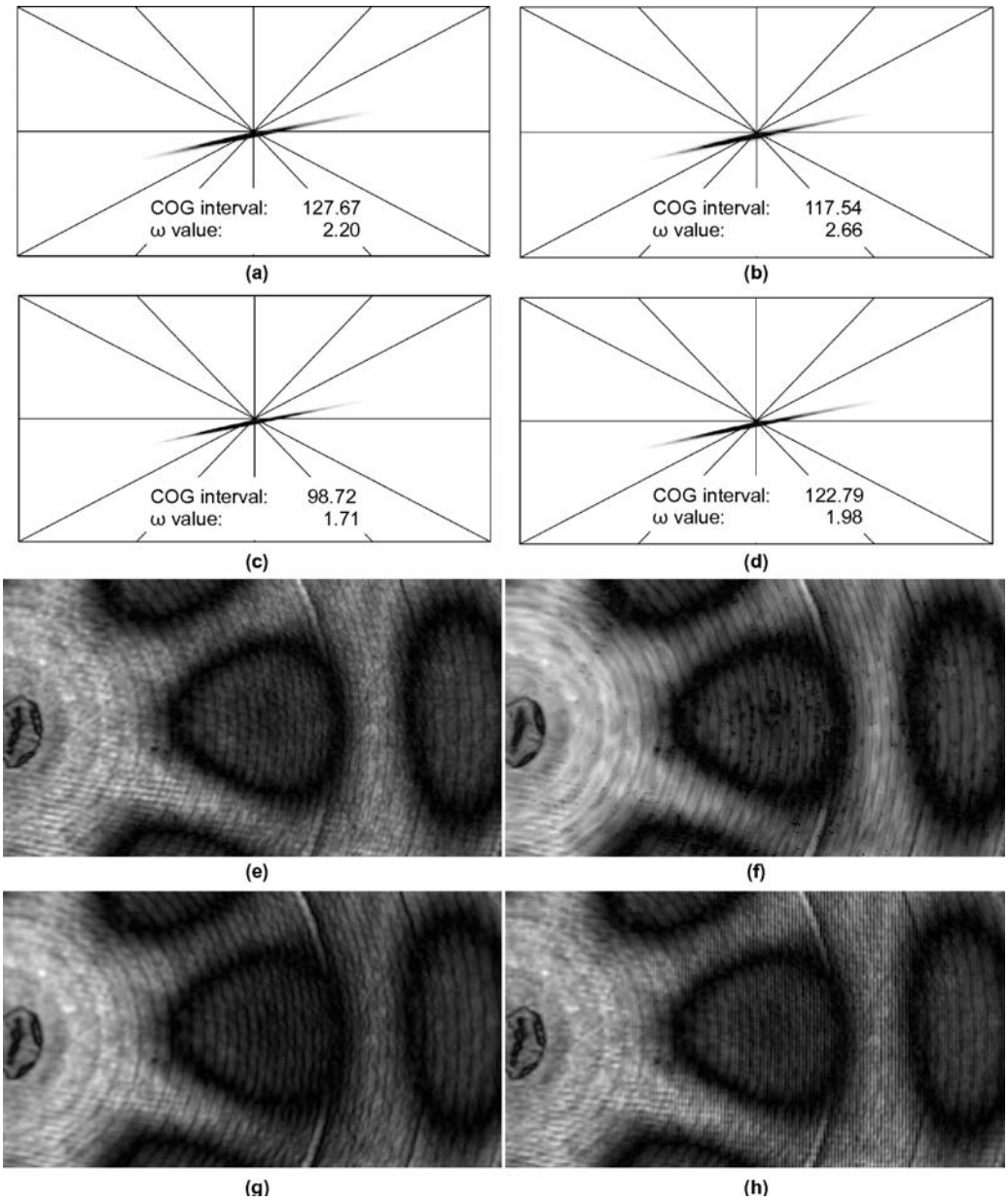

Fig. 6. Lattice site representations of the same set of interferograms, but with different algorithms used: (a) no denoising algorithm – all parameters are treated as reference values, (b) spin filtering, the first variant (see Sect. 2.1), (c) spin filtering, the second variant (see Sect. 2.1), and (d) wavelet thresholding at the first level. (e)-(h) intensity modulation maps corresponding to the above mentioned algorithms.

framed in order to visually assess experimental imperfections and also to compute the parameters needed, the distance between the positive and negative centres of gravity and the ω parameter.

The effects of those actions can be examined in Fig. 6.

Looking at Figs. 6(a) and 6(e) one can notice that the fringe pattern used does not contain much noise (small visual spread and ω value) and the experimental imperfections are negligible (straight line). In this case, the filtering technique has to be very exact. The first type of spin filtering has effectively made the interferogram worse, the ω value has increased and the interval has shrunk by 10. The reason for this is a limited number of directions used in this method. As for Figs. 6(c) and 6(g), where the second variant of spin filtering is shown, one could state that this denoising technique is the best because it gives the smallest $\mathring{u}$ parameter. However, that is not exactly true as this method has also the lowest interval, this corresponds to a dampening nature of the 1D averaging that was used in the algorithm.

In Figs. 6(d) and 6(h), the value ω is slightly worse than for the best spinning filter, but the interval is the best of all three methods. This is due to the fact that properly applied wavelet thresholding changes the information locally and not globally like the other methods, thus realizes filtering in a more efficient way. One has to remember that this is the best result achieved by using decomposition level one, the performance on other levels of decomposition is shown in Table 1.

Table 1. Performance of denoising operation with wavelet thresholding depending on decomposition level applied.

Decomposition level	1	2	3	4	5	6	7	8	9	10
COG interval	122.79	104.89	97.46	96.9	96.67	96.73	96.69	96.68	96.56	96.55
ω parameter	1.98	2.71	2.98	3.01	3.03	3.04	3.05	3.03	3.04	3.04

The relationship between Table 1, the experimental data and Fig. 5 depicting simulation data is obvious. One could ask – why? The cause is obvious when one important feature of a wavelet thresholding is realized, strong thresholding can lead to data compression rather than denoising [2,20,21] and in that case the error grows (normal situation in lossy compression). The chosen regions of an interferogram and a modulation map in Fig. 7 show clearly the compression effect. Notice the increasing roughness of the curved fringes while the decomposition level is increasing, the fringe modulation is also degrading.

Due to the fact that in this paper, till now, the lattice site representation has not been used to estimate filtering performance of various denoising algorithms, the additional phase deviation calculations have been made to further support the conclusions drawn in the first part of this section. A set of five interferograms was preprocessed with the algorithms discussed. The resulting sets were used to calculate phase distribution employing the classic Schwider-Hariharan five-frame algorithm [19]. Next, the phases were unwrapped by the quality guided algorithm [22] (φ_F, in Table 2) and subtracted from a reference surface (Ref_{Surf}, in Table 2) that was created by averaging multiple interpolations of a random grid points of non-preprocessed, unwrapped phase distribution. Table 2 shows the final phase distribution deviation introduced by the examined algorithms. As it can be noted, all the filtering properties that were discussed in the beginning of this section have shown as cumulated phase distortion, effectively making the wavelet algorithm the most accurate in this case. On the other hand, the dampening nature of the spin filters has prevailed over their accuracy in noise-removal, worsening the overall phase distribution results.

5.3. Execution time

Properly implemented denoising using wavelet thresholding algorithm gives not only better results in comparison to spin filtering techniques but is also less time consuming. Typically, the wavelet denoising is computed roughly with the same speed as a simple variant of spin filtering (having better accuracy than the more complicated one) mainly due to a very straightforward implementation of the DWT procedure. More precise variant of spin filtering takes roughly 40 times more than the other algorithms to complete the calculations. In this case, the most time-consuming part is the plane fitting to a neighbourhood matrix which in turn enables us to estimate the fringe tangential direction.

6. Final conclusions and recommendations

Out of the two types of denoising methods presented in this paper, the wavelet denoising by thresholding is recommended since it not only enables us to achieve good denoising effects but also almost preserves the initial data frequency bandwidth. The algorithm is not time-consuming which is

Table 2. Influence of denoising operations on a phase distribution error.

Denoising technique	No denoising	Spin filtering, 1st variant	Spin filtering, 2nd variant	Wavelet thresholding
Median $\left(\left\|\varphi_F - Ref_{Surf}\right\|\right)$ (rad)	0.34	0.54	0.52	0.32

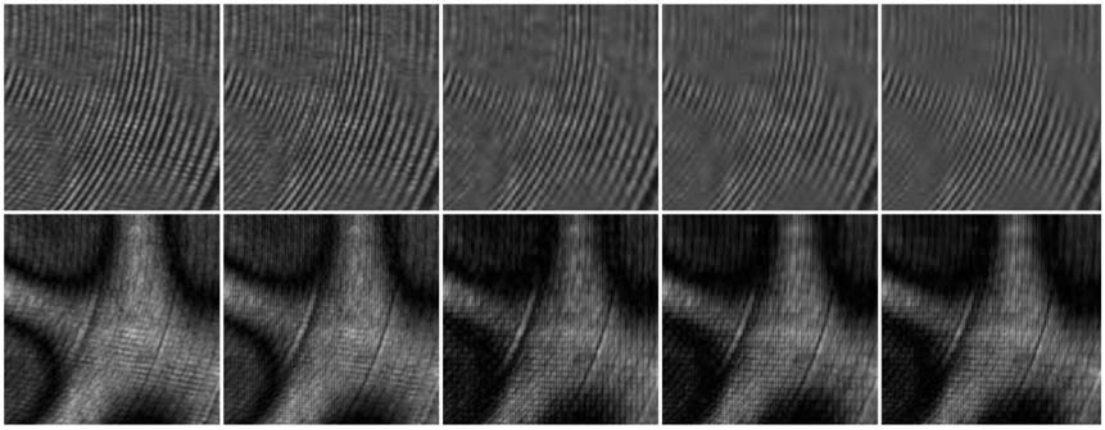

Fig. 7. Comparison between a non-denoised area and areas denoised by a wavelet thresholding with decomposition levels varying from one to four (image order from left to right). Notice the increasing influence of compression due to excessive thresholding.

equally important. By the use of this algorithm one can conduct high accuracy interferometric measurements.

The issues that need to be addressed in continued research include automatic determination of the decomposition level (the use of one of the two lattice site parameters discussed in this paper is considered), an adaptation of a lattice site representation to only two phase-shifted interferograms (the computation of a lattice site representation from five phase-shifted interferograms puts a dependence on even phase-shifts), further simulations to compare the experimental lattice site representations with the artificial ones.

Acknowledgments

Authors would like to thank Adam Styk for his work on the spin filtering technique, the access to the source code and many valuable comments regarding lattice site representation and last but not least, an anonymous reviewer for helpful remarks. This work was supported by the Ministry of Science and Higher Education grant no. 0579/T02/2007/32 and statutory activity funds.

The works described in Ref. 12 were co-supported by EU Project OCMMM (the part of experiments was performed at Laboratoire d'Optique P. M. Duffieux, Université de Franche-Comté, Besançon, France).

This paper is a revision of the paper presented at the 16th Polish-Czech-Slovak Conference on Wave and Quantum Aspects of Contemporary Optics, September 2008, Polanica Zdrój, Poland. The paper presented there appears unrefereed in *Proc. SPIE* **7141**.

References

1. D.W. Robinson and G.T. Reid, *Interferogram Analysis: Digital Fringe Pattern Measurement Techniques*, Taylor & Francis Ltd, London, 2002.
2. D.L. Donoho, "De-noising by soft-thresholding", *IEEE T. Inform. Theory* **41**, 613–627 (1995).
3. Q.F. Yu, "Spin filtering processes and automatic extraction of fringe centerlines in digital inteferometric patterns", *Appl. Opt.* **27**, 3782–3784 (1988).
4. Q. Yu, X. Liu, and K. Andresen, "New spin filters for interferometric fringe patterns and grating patterns", *Appl. Opt.* **33**, 3705–3711 (1994).
5. A. Styk and K. Patorski, "Identification of nonlinear recording error in phase shifting interferometry", *Opt. Lasers Eng.* **45**, 265–273 (2007).
6. K. Patorski, A. Styk, L. Bruno, and P. Szwaykowski, "Detection and assessment of the nonuniform phase displacement error in temporal phase shifting interferometry", *Opt. Express* **14**, 5232–5249 (2006).
7. P. Goupillaud, A. Grossman, and J. Morlet, "Cycle-octave and related transforms in seismic signal analysis", *Geoexploration* **23**, 85–102 (1984).
8. Q. Kemao, "Windowed Fourier transform for fringe pattern analysis", *Appl. Opt.* **43**, 2695–2702 (2004).
9. J.P. Antoine, R. Murenzi, and S.T. Ali, *Two-dimensional Wavelets and their Relatives*, Cambridge University Press, Cambridge, 2004.
10. I. Daubechies, *Ten Lectures on Wavelets*, SIAM, Philadelphia, 1992.
11. D.L. Donoho and I.M. Johnstone, "Ideal spatial adaptation by wavelet shrinkage", *Biometrika* **81**, 425–455 (1994).
12. L. Salbut, K. Patorski, M. Jóźwik, J. Kacperski, C. Gorecki, A. Jacobelli, and T. Dean, "Active micro-elements testing by interferometry using time-average and quasistroboscopic techniques", *Proc. SPIE* **5145**, 23–32 (2003).
13. K.G. Larkin, "Efficient nonlinear algorithm for envelope detection in white light interferometry", *J. Opt. Soc. Am.* **A13**, 832–843 (1996).
14. A. Styk and K. Patorski, "Analysis of systematic errors in spatial carrier phase shifting applied to interferogram intensity modulation determination", *Appl. Opt.* **46**, 4613–4624 (2007).
15. K. Patorski, Z. Sienicki, and A. Styk, "The phase shifting method contrast calculations in time average interferometry error analysis", *Opt. Eng.* **44**, 065601 (2005).
16. K. Patorski and A. Styk, "Interferogram intensity modulation calculations using temporal phase shifting: error analysis", *Opt. Eng.* **45**, 085602 (2006).
17. B. Gutman and H. Weber, "Phase-shifter calibration and error detection in phase-shifting applications: a new method", *Appl. Opt.* **37**, 7624–7631 (1998).
18. T. Kreis, *Handbook of Holographic Interferometry*, Wiley-VCH Verlag GmbH & Co. KGaA, Weinheim, 2005.
19. J. Schwieder, R. Burow, K.-E. Elsser, J. Grzanna, R. Spolarczyk, and K. Merkel, "Digital wave-front measuring interferometry: some systematic error sources", *Appl. Opt.* **22**, 3421–3432 (1983).
20. M. Hansen and B. Yu, "Wavelet thresholding via MDL for natural images", *IEEE T. Inform. Theory* **46**, 1778–1788 (2000).
21. A. Buades, B. Coll, and J.M. Morel, "A review of image denoising algorithms, with a new one", *Multiscale Model. Sim.* (*SIAM*) **4**, 490–530 (2005).
22. D.C. Ghiglia and M.D. Pritt, *Two-Dimensional Phase Unwrapping: Theory, Algorithms and Software*, Wiley-Interscience, New York, 1998.

